



A salt-derived solid electrolyte interphase by electroreduction of water-in-salt electrolyte for uniform lithium deposition

Zhenxing Wang^{a,b,1}, Hengguo Sun^{c,1}, Jingchi^a, Yulai Li^a, Inwei Wei^{a,b}, Yin Li^{a,b}, Zhenhua Sun^{a,b}, Gaigang An^c, Cheng Li^{a,b,c}

^a Shenyang National Laboratory for Materials Science, Institute of Metal Research, Chinese Academy of Sciences, 72 Wenhua Road, Shenyang, 110016, China

^b School of Materials Science and Engineering, University of Science and Technology of China, Hefei, 230026, China

^c School of Chemical Engineering, University of Science and Technology Liaoning, Anshan, 114051, China

- The concept of salt-derived solid electrolyte interphase is proposed
- This film is rich in inorganic components mainly Li_2CO_3 and LiF
- This film greatly reduces the overpotential and facilitates fast Li^+ transport
- High coulombic efficiency and uniform spherical Li deposition are achieved
- This work emphasizes the functions of salt decompositions on protection of Li

A

A

A

Keywords:

Water-in-salt
solid electrolyte interphase
dendrite-free Li anode
electroreduction
space charge

Notorious growth of dendritic lithium with low coulombic efficiency causes safety and stability issues, which hinder practical applications. To control the lithium deposition so that one has a dendrite-free lithium metal anode with high coulombic efficiency is highly desirable but challenging. Here, this work reports a copper substrate covered by a salt-derived solid electrolyte interphase that produced by electroreduction of a highly concentrated water-in-salt electrolyte to realize stable lithium deposition quite distinct from the resistive layer comprised principally of solvent-derived organic species such as lithium alkyl carbonates that produced in conventional dilute electrolyte, this salt-derived solid electrolyte interphase is rich in inorganic components mainly Li_2CO_3 and LiF , which effectively reduce the overpotential and facilitate fast Li^+ transport. In addition, a small number of reduced fluorine organic anions - F^- stabilize the space charge to give a uniform distribution of Li^+ . Such a solid electrolyte interphase on the copper substrate is able to modulate the lithium plating/stripping to produce uniform spherical lithium deposition with no dendrites, and a high coulombic efficiency $\approx 100\%$ is achieved. This work provides a unique strategy to enlarge the functions of the lithium salt decompositions on the protection of lithium metal anodes.

1. Introduction

Lithium-ion batteries (LIBs) have achieved great success for use in portable devices and electric vehicles, but are unable to meet the currently ever-increasing demands of energy density [1]. The fact that the Li metal, with a specific capacity of an order of magnitude greater than that of the state-of-the-art Li anode, has attracted great interest in

achieving rechargeable batteries with a higher energy density [2]. However, there is still a long way to go before the practical application of Li metal due to its poor safety, low coulombic efficiency [3] and short lifespan, its parasitic reactions with liquid electrolytes, and unstable and uncontrollable dendritic electrodeposition [4].

Such unsolved issues are associated with the high activity of Li metal [5]. Li metal, which has the most negative electrochemical potential

Corresponding author. Shenyang National Laboratory for Materials Science, Institute of Metal Research, Chinese Academy of Sciences, Wenhua Road, Shenyang, 110016, China.

E-mail address: zhenxingwang@imr.ac.cn (Z. Wang).

¹ These authors contributed equally to this work.

<https://doi.org/10.1016/j.jpowsour.2019.08.011>

Received 1 March 2019; received in revised form July 2019; Accepted August 2019

Available online 5 September 2019

0378-7753/© 2019 Elsevier B.V. All rights reserved.

– vs a standard hydrogen electrode, can react spontaneously with all polar aprotic solvents. When fresh metal is exposed to the electrolyte, an electrically insulating but ionically conducting solid electrolyte interphase (SEI) is

interfacial electrochemical process on the electrode surface. Recently, the emerged concept of water-in-salt electrolyte has been used to expand the electrochemical window of salts. At room temperature, the maximum solubility of universal lithium salt in water is about 1 M. At concentrations of lithium above 1 M, the reduction potential of Li^+ is altered by its interaction with H_2O . Aggregates such as $\text{Li}_x\text{H}_y\text{O}_z$ become unstable below 1 M vs Li^+/Li , which is higher than the reduction potentials of 1 M for isolated Li^+ and H_2O for hydrogen both vs Li^+/Li in such an electrolyte, a dense Li film dominated with Li_2O is formed as a result of reduction of the Li^+ by the Li^+ solvation sheath, which prevents further sub-reactions.

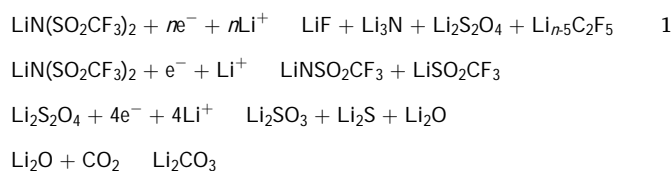
Following this concept, we reported an electroreduction route to construct an artificial inorganic-rich Li film derived from reduced salt anions on a Cu substrate (Fig. 1) in a typical three-electrode cell (Fig. 1), a Cu foil as the working electrode was immersed in the water-in-salt electrolyte, and cyclic voltammetry scans were then performed in the range 1 M vs Li^+/Li with a scan rate of 1 mV s⁻¹ for 10 cycles. The experimental details are available in Materials and Methods.

After pre-processing, the Cu foil was covered by a dense interphase with a large number of nanoparticles (Fig. 1a and b). More importantly, the cross-view image of the Cu with the Li film showed that a thin Li film composed of nanoparticles covered on Cu surface (Figs. 1b-c), which were composed of Li_2O and Li_2CO_3 elements (Figs. 1d-f). A transmission electron microscopy image clearly showed that the Cu substrate was decorated by nanoparticles of few to tens of nanometers size (Fig. 1c and Fig. 1g). High-resolution images of the Li film showed the crystal lattice of the nanoparticles, corresponding to inorganic products Li_2O and Li_2CO_3 (Fig. 1d). Energy-dispersive X-ray spectroscopy analysis also demonstrated that Li , C , and O were evenly distributed on the Cu substrate (Fig. 1e-i). To probe the chemical composition of the Li film on the Cu substrate, X-ray photoelectron spectroscopy was carried out. The surface of bare Cu using a Cu half cell in 1 M LiClO_4 electrolyte after 10 cycles was also characterized by the strong signal detected in the 1s spectrum between 285 and 295 eV, which can be assigned to C or C_xO_y species (Fig. 1a). The peaks in the 1s spectrum detected at 1.5, 1.0, 1.0 and 1.0 eV corresponded to Li , Li , Li and Li (Fig. 1b), respectively. The inorganic species Li_xO_y , Li_2O and Li_2CO_3 accounts for 100% for the organic species according to the peak area. In contrast, the solvent-derived solid electrolyte interphase on bare Cu is principally composed of organic C_xO_y species. Almost 100% of the 1s spectrum (Fig. 1c), inorganic species Li , Li and Li in Li accounts for 100% based on the peak area (Fig. 1c). The detected signals of Li were mainly from two species: a few fluorine organic anions C_xF_y at ≈ 1.5 eV originating from partially reduced

fragments, and dominant Li at ≈ 1.0 eV. In addition, the proportion of Li in the Li film accounts more than the solvent-derived Li film on bare Cu based on the ratio of peak area. Here, Li , Li , and Li are considered as the main species in the Li film and normalization processing is carried out. As the Table 1 shows, the ratio of inorganic species in the salt-derived Li film is far greater than that in the solvent-derived Li film, atomic ratio here, therefore, we conclude that the Li film is rich in inorganic components mainly Li_xO_y and Li_2CO_3 than the solvent-derived Li film. As previous reports, on one hand, Li is a good electrical insulator ($\approx 10^{-11}$ cm⁻¹) to prevent electrons from crossing the Li film. On the other hand, Li has been demonstrated to greatly suppress dendritic Li growth due to its high surface diffusivity for Li^+ . One of the inorganic products was a decomposition product of residual salts caused by γ -ray radiation (Fig. 1g). Therefore, the Li film is principally composed of inorganic Li_xO_y and Li_2CO_3 species, accompanied by a small amount of organic C_xO_y . The chemical composition of the Li film was also investigated using time-of-flight secondary ion mass spectrometry (ToF-SIMS) in both negative and positive modes. Several negative species were detected (Fig. 1e), including Li^- ($m/e=1$), Li_2^- ($m/e=2$), Li_3^- ($m/e=3$) and Li_4^- ($m/e=4$). In particular, the signal from Li^- species was much stronger than from other species, which illustrated the high content of Li in the Li film. The positive mode of ToF-SIMS was also measured under the same conditions and a positive cluster species Li^+ ($m/e=7$) was observed (Fig. 1f). To estimate the thickness of the Li film, we conducted Li^+ sputtering to obtain a depth profile (Fig. 1g). As the sputtering time increased, the signal of the detected species all went down. Even that Li and C represented the components of the Li film, their declining trend suggested that the average thickness of the Li film was ≈ 1 nm ($t = 1$ s and sputtering rate = 1 nm s⁻¹).

The electrochemical pre-processing was performed under air atmosphere to exclude the interference of gases like O_2 , we performed control experiments under an Ar atmosphere. Similar to the results under air, a series of inorganic products, such as Li_2O , Li_2CO_3 , $\text{Li}_2\text{S}_2\text{O}_4$, Li_2SO_3 , Li_2S , Li_2O , Li_2CO_3 , were generated (Fig. 1g), the main difference being the absence of Li_2CO_3 under Ar atmosphere. Surface-enhanced Raman spectra for the Li film also confirmed that the Li_2CO_3 generated was associated with Li_2CO_3 . Meanwhile, active species in Raman spectra, such as Li_2O centered near 1000 cm⁻¹ and $\text{Li}_2\text{S}_2\text{O}_4$ at 1000 cm⁻¹ were detected. This result is consistent with the results. Detailed analyses are given in the supporting information.

Combining the above results and analyses, the Li film on the Cu substrate was generated by the electrochemical pre-processing and consisted of reductive decomposition products of the Li . Whether annealed under Ar or air atmospheres, the main reduced products of Li are Li_2O and Li_xO_y , accompanied by a small amount of C_xO_y . The formation mechanisms of the Li film are as follows:



The Li film obtained by electrochemical processing is distinct from the conventional Li film formed in a non-aqueous electrolyte (Fig. 1). The conventional passivated Li film is principally composed of solvent-derived organic species like C_xO_y . Li^+ move sluggishly through the organic species by pore diffusion, which produces a low ionic conductivity and an uneven charge distribution. The non-uniform Li^+ flux and local high concentrations of Li^+ accelerate the growth of Li dendrites and consumption of the electrolyte. Rather than a highly resistive layer, this new Li film is largely inorganic, mainly Li_xO_y and Li_2CO_3 with a small number of fluorine organic anions C_xF_y .

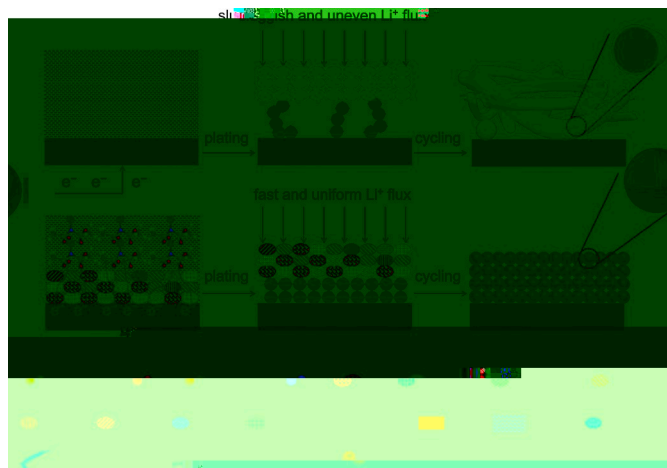


Fig. 1. Schematics of the Li plating behavior on different substrates.

provide superior ionic conductivity and fast i^+ diffusion, the abundance of i^- , with a high surface energy, produces a small interfacial resistance and uniform spatial distribution of i^+ , also suppressing dendritic i^- growth. In addition, the i^- species inhibit space charge accumulation, which induces a homogeneous i^+ distribution and facilitates homogeneous i^- deposition [1]. As the plating process proceeds, the i^- film facilitates the fast and uniform deposition of spherical i^- particles, resulting in a stable cycling performance. The i^- plating behavior on the Cu substrate with the i^- film was evaluated in a coin cell. Bare Cu substrate was the controlled

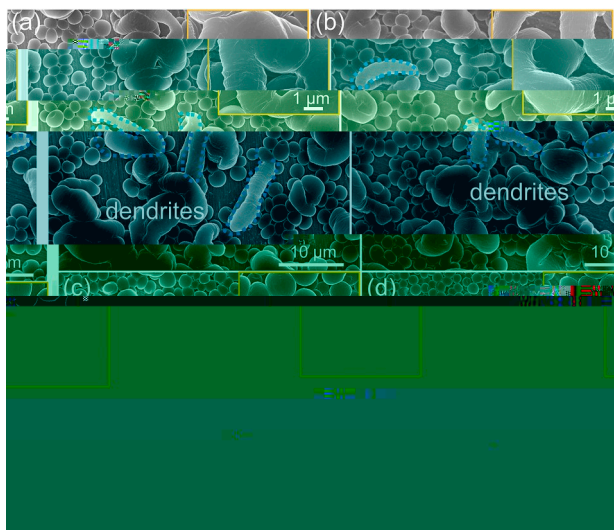


Fig. 4. Morphologies of the 1st Cu nuclei on bare Cu substrate and the Cu substrate with 1 nm SDSEI. (a) SEM images of Cu nuclei on the bare Cu substrate at 1 mA cm⁻². (b) SEM images of Cu nuclei on the Cu substrate with the 1 nm SDSEI at 1 mA cm⁻². (c) SEM images of Cu nuclei on the bare Cu substrate at 1 mA cm⁻². (d) SEM images of Cu nuclei on the Cu substrate with the 1 nm SDSEI at 1 mA cm⁻². The insets are high-magnification images of the Cu nuclei.

rised to a relatively stable voltage plateau at -0.28 V vs i⁺, which was the mass-transfer-controlled overpotential. The nucleation overpotential is defined as the difference between the minimum voltage and the later stable mass-transfer-controlled overpotential, which was 1 mV for a bare Cu substrate. In contrast, the curve of the Cu substrate with the 1 nm SDSEI had a much smaller voltage minimum of -0.28 V vs i⁺ at the nucleation stage, with a nucleation overpotential of only 2 mV. The mass-transfer overpotential depends on the applied current density and the migration properties of the i⁺. At the same current density of 1 mA cm⁻², the Cu substrate with the 1 nm SDSEI had a smaller mass-transfer overpotential of 2 mV compared to 1 mV for bare Cu. The lower mass-transfer controlled overpotential indicated that the 1 nm SDSEI effectively improved the electrodeposition kinetics. Electrochemical impedance spectroscopy analysis of

the cells was conducted to illustrate the kinetic behavior of the anodes. Fig. 5(b) shows Nyquist plots had a semicircle in high frequency region, which was ascribed to i⁺ migration through the 1 nm SDSEI on the electrode surface. If the average thickness of the 1 nm SDSEI is about 1 nm, a high i⁺ conductivity of 1 × 10⁻¹⁰ cm⁻¹ is achieved by the 1 nm SDSEI, around two times higher than bare Cu (1 × 10⁻¹¹ cm⁻¹). The good conductivity of i⁺ migration through the 1 nm SDSEI contributes to a fast i⁺ transport kinetics.

To further investigate the reliability of the Cu substrate with the 1 nm SDSEI, the cycle life of the Cu plating stripping was analyzed in Cu cells with 1 mA h cm⁻² of pre-deposited Cu. The cut-off voltage of recharge was fixed at 1 V vs i⁺. The electrochemical performance of different thicknesses of SDSEI on Cu substrate was evaluated in Fig. 5(c). As the increasing number of pretreatment, the thickness of the SDSEI gradually reached to a maximum of approximately 1 nm when the SDSEI is too thick to transport electrons. In accordance with the thickness of the SDSEI, the initial Coulombic efficiency was increased from 60% to 90%. Higher than the bare Cu, the Coulombic efficiency for the Cu substrate with the 1 nm SDSEI gradually increased to 90% after several cycles and remained stable for 100 cycles. Fig. 5(d) shows the high Coulombic efficiency can be attributed to the 1 nm SDSEI which effectively reduces side reactions between the deposited Cu and the electrolyte. After increasing the current density to 1 mA cm⁻², Fig. 5(a) shows the initial Coulombic efficiency of the Cu substrate with the 1 nm SDSEI exhibited 100%, which exceeded the Cu substrate. And then the Coulombic efficiency increased to a high average value of 90% over 100 cycles without failure, even at a high current density of 1 mA cm⁻². Fig. 5(b) shows the Cu plating stripping was stable without fluctuation. However, cells with the bare Cu substrate showed a rapid loss of performance after 10 cycles at 1 mA cm⁻² and 100 cycles at 1 mA cm⁻². To observe the Cu deposition morphologies, we disassembled the Cu cells after 100 cycles. A large number of Cu dendrites with sharp tips had formed at different current densities. Fig. 5(d) and Fig. 5(e) show irregular and random Cu growth, increased contact area with the non-aqueous electrolyte, further consumed active Cu metal and electrolyte, producing a low Coulombic efficiency. As a comparison, the plated Cu with 1 nm SDSEI became larger and thicker while maintaining the spherical morphology of the Cu even after plating stripping cycles. Fig. 5(f) and Fig. 5(g) show these different results confirm that the 1 nm SDSEI produces uniform Cu deposition without Cu dendrites.

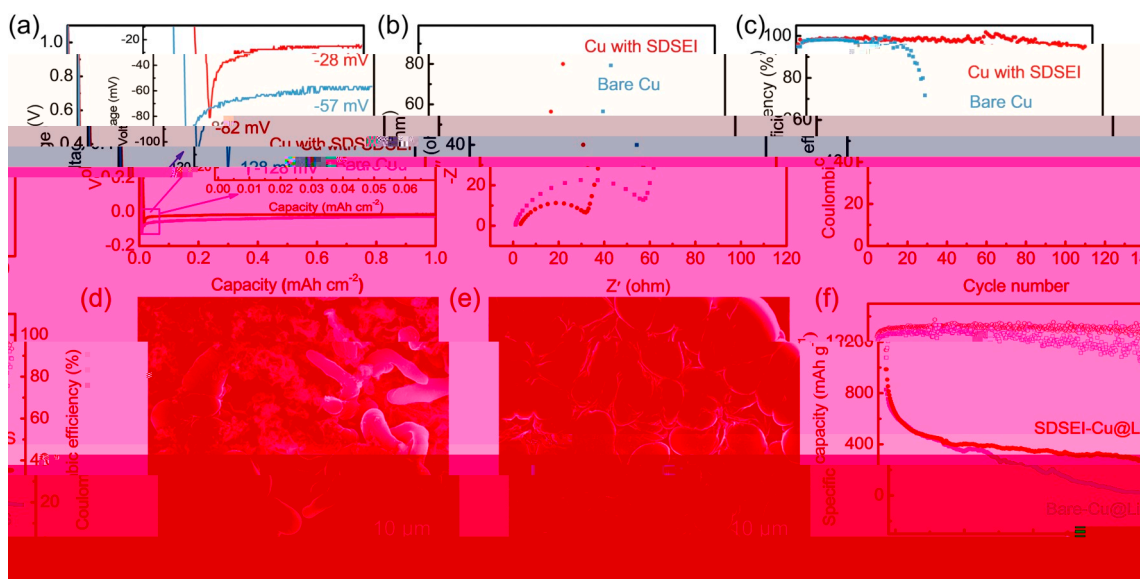


Fig. 5. Electrochemical performance of Cu cells. (a) Voltage-time curves after the 1st Cu nucleation at 1 mA cm⁻². (b) Nyquist plots of Cu cells after the 1st cycle at 1 mA cm⁻². (c) Coulombic efficiency (%) of Cu deposited on bare Cu substrate and the Cu substrate with the 1 nm SDSEI. The cells were tested with a fixed areal capacity of 1 mA h cm⁻². (d) SEM image of the Cu morphology on the bare Cu substrate and (e) the Cu substrate with the 1 nm SDSEI. (f) Electrochemical performance of Cu cells with 1 mA h cm⁻² of pre-deposited Cu. (g) SEM image of the Cu morphology on the bare Cu substrate and (h) the Cu substrate with the 1 nm SDSEI.

i- full cells were assembled to verify the advantages of the above strategy for practical use with mAh cm^{-2} of pre-deposited Ni cells based on the Cu substrate with the Ni and the bare Cu substrate are denoted as Cu/Ni and Cu, respectively. The Cu/Ni cell exhibited a C_d of about 1 in the first cycles. However, beyond 10 cycles, it quickly dropped to 0.5, accompanied by a fast